Journal of Materials Chemistry B

ROYAL SOCIETY OF CHEMISTRY

PAPER

View Article Online
View Journal | View Issue

Cite this: J. Mater. Chem. B, 2022, 10, 2570

Fibrillated bacterial cellulose liquid carbene bioadhesives for mimicking and bonding oral cavity surfaces†

Juhi Singh, [ab] Terry W. J. Steele *[c] and Sierin Lim *[b]

Received 16th September 2021,
Accepted 25th November 2021

DOI: 10.1039/d1tb02044g

rsc.li/materials-b

Topical treatments for oral wounds and infections exhibit weak adhesion to wet surfaces which results in short retention duration (6–8 hours), frequent dosing requirement and patient incompatibility. To address these limitations, aqueous composites made of fibrillated bacterial cellulose and photoactive bioadhesives are designed for soft epithelial surfaces. The aqueous composites crosslink upon photocuring within a minute and exhibit a transition from viscous to elastic adhesive hydrogels. The light-cured composites have shear moduli mimicking oral mucosa and other soft tissues. The tunable adhesion strength ranges from 3 to 35 kPa on hydrated tissue-mimicking surfaces (collagen film). The results support the application of bacterial cellulose hydrogel systems for potential treatment of mucosal wounds.

Introduction

According to the Global Burden of Disease Study 2017, chronic oral diseases affect about 45% of the world's population.[1] Oral non-communicable diseases are expressed in the oral cavity in the form of wounds, ulcers or lesions.[2,3] Mucoadhesives based on polymer entanglement have limited retention times due to unchecked swelling leading to loss of structural integrity and delamination, resulting in multiple reapplications and poor patient compliance.[4–7] Low-risk approaches have relied on mucoadhesive swelling for entanglement of mucin on epithelial surfaces.[4] This provides transient fixation, but unchecked water absorption yields poor cohesive (storage modulus 0.01-0.1 kPa)[5,8–12] and adhesion strength (2–5 kPa[13–15] at 2 cm^2). Chemical curing strategies based on catechols achieve a flexible storage modulus (0.01–0.1 kPa) and higher adhesion strength compared to mucoadhesives, but require 6–10 min of static loads before tack strength can develop.[16–18] Faster acting mechanisms are required for rapid placement and to extend tissue fixation.

Previous investigations on layered composites of bacterial cellulose (BC) films and PAMAM-*g*-diazirine (PDz) (referred to as BC_PDz(lc), lc represents layered composites) yielded moderate adhesion strength (7–17 kPa) that withstood days of aqueous shear strain.[19] The long-term fixation is attributed to the combination of PDz-mediated covalent bonding and BC's hydration-resistant cohesive strength. The epithelial sloughing every 5–6 days can lead to natural release of the layered composite.[20] Diazirine groups present in the PDz generate reactive crosslinking groups (carbenes) upon photocuring or electrocuring.[21,22] The photocured PDz composites with solute concentration of 50% or greater have adhesion strength of 5–45 kPa against wet tissue substrates.[23–27] The high PDz concentration leads to high cationic density and subsequently osmotic imbalance and cytotoxicity.[28,29] Hence, lower solute concentrations are desired. It is hypothesized that incorporation of BC will yield composites capable of crosslinking at lower solute concentrations. In addition, the applicability of PDz and BC-based materials may be further expanded if BC_PDz biocomposite is reformatted from film to viscous form or hydrogel that allows liquid dispensing on irregular surfaces followed by UV light curing for fixation.

BC is a naturally derived hygroscopic polymer from *Aceto-bacteraceae* family members,[30] which exhibits controlled hydration and stable cohesive strength as a thin film, thus balancing the osmotic imbalance of PDz bioadhesives.[31] This inherent self-regulating water absorption ability of BC can be advantageous for moist environments such as oral cavity. BC is sold commercially as a food product, *Nata de coco*,[32] attesting to low biotoxicity risks and ease of large-scale industrial production. Based on their properties, it is hypothesized that composites of

[a] NTU Institute for Health Technologies, Interdisciplinary Graduate Program, Nanyang Technological University, 61 Nanyang Drive, 637335, Singapore. E-mail: juhi003@ntu.edu.sg
[b] School of Chemical and Biomedical Engineering, Nanyang Technological University, 70 Nanyang Drive, Block N1.3, 637457, Singapore. E-mail: SLim@ntu.edu.sg
[c] School of Materials Science and Engineering (MSE), Division of Materials Technology, Nanyang Technological University (NTU), 639798, Singapore. E-mail: WJSteele@ntu.edu.sg

† Electronic supplementary information (ESI) available. See DOI: 10.1039/d1tb02044g

fibrillated BC and PDz would reduce the % solute of PDz cross-linker required while yielding elastic films upon photocuring. The photocured composites are expected to exhibit viscoelastic dissipation due to the dual hybrid network provided by the PDz dendrimer dissolved in BC linear chains. To assess the hypotheses, structure–activity relationships of BC_PDz aqueous composite (referred to as BC_PDz(h), h represents hydrogel) is evaluated for dynamic viscosity, photocuring rheology, morphological analysis, crosslinking mechanism, and lap shear adhesion strength with respect to total solute percentage and UV dose.

Experimental

Materials

Polyamidoamine (PAMAM) dendrimer, Generation 5, M_w = 28.8 kDa was bought from Dendritech, Inc., USA. 3-[4-(Bromomethyl)phenyl]-3-(trifluoromethyl)-diazirine(bromo-diazirine) was purchased from TCI, Japan. All other chemicals were purchased from Sigma Aldrich, unless specified otherwise.

Methods

Strains and culture medium. *Gluconacetobacter hansenii* ATCC 53582 was employed for the fermentation of BC in Hestrin–Schramm (HS) medium. HS medium was composed of glucose (20 g L^{-1}, 0.11 M), citric acid monohydrate (1.15 g L^{-1}, 0.005 M) and Na_2HPO_4 (2.7 g L^{-1}, 0.02 M) enriched with yeast extract (5 g L^{-1}) and peptone (5 g L^{-1}) with final pH 4.5. Media was prepared and autoclaved at 120 °C for 15 min before use.

Microbial fermentation. *G. hansenii* ATCC 53582 was grown overnight in media (HS medium) for 24 hours in shaking conditions at 26 °C to produce the inoculum. The pellicle production was started with the inoculum at 5% (v/v) and cultured in 24-well plates at 26 °C for 5 days. The BC pellicles were harvested and washed with distilled water followed by sodium hydroxide treatment (0.25 N) for 30 minutes at 60 °C for removal of bacterial cells. The pellicles were then washed thoroughly with deionized water. BC produced and harvested after 5 days was further employed for formulating fibrillated dispersion.

Synthesis of PAMAM-*g*-diazirine. Grafting of diazirine to PAMAM backbone was performed as previously reported by Feng *et al.*[23] The structure–activity relationships of PDz have been evaluated with respect to dendrimer generation, diazirine grafting degree, concentration, toxicity, and on-demand activation in previous reports.[23,26,33–35] PAMAM-*g*-diazirine with 20% conjugation was employed for further experiments.

Formulation of BC_PDz hydrogels (BC_PDz(h)). BC_PDz(h) composites were formulated as depicted in Fig. 1. Washed BC films were cut into pieces and suspended in deionized water. The obtained dispersion was sonicated for 3 hours at 37% amplitude with 10 s on, 10 s off cycle (Vibra-Cell™, VCX 500, SONICS®). The BC dispersion was then centrifuged (11 180 × *g* force, Thermo Scientific™ Sorvall™ Legend™ XTR Centrifuge) to remove excess water. A typical BC hydrogel concentration was 1.3 ± 0.2% (w/w). Different compositions of BC_PDz(h) were prepared by mixing varying amounts of BC and PDz, as mentioned in Tables 1 and 2 and magnetically stirred to ensure

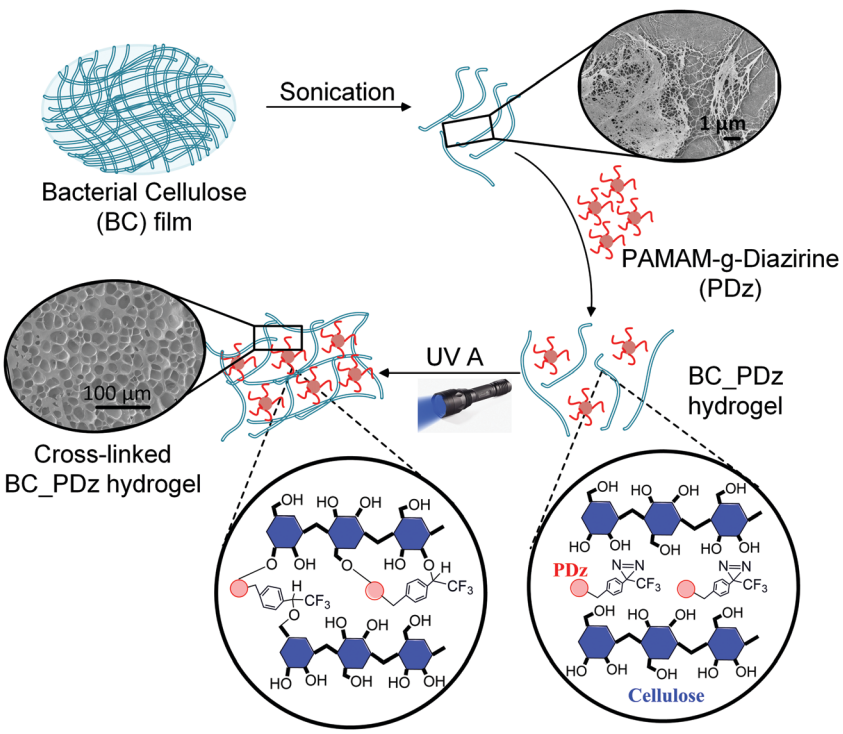

Fig. 1 Schematic representation of BC_PDz(h) production. BC pellicles are sonicated to obtain hydrogel. Hydrogel (1.3% w/v) is then mixed with PDz to obtain BC_PDz(h) composite hydrogel; followed by covalent insertion with cellulose macromolecules upon photocuring.

Table 1 Material properties of BC_PDz(h) formulations before and after curing at varying %total solute

Total solute%[a] (w/w)	PDz% w/w (mM)	BC% w/w (mM)	[Diazirine]/[OH] mol ratio[b]	G' before curing (kPa)	G' max at UV off (kPa)	Gelation UV dose (J)	Uncured state[c]
10	9.0 (2.4)	1.0 (80)	0.13	0.5 ± 0.3	1.6 ± 0.2	3.2 ± 0.3	Bingham Plastic
20	19.0 (6.5)	1.0 (80)	0.35	1.7 ± 0.3	3.2 ± 0.5	2.6 ± 0.7	Bingham Plastic
33.3	32.5 (13.5)	1.0 (80)	0.7	3.3 ± 1.1	8.9 ± 2.1	2.3 ± 0.8	Viscous

[a] Total solute% = (PDz% w/w + BC% w/w) M_w of PDz = 36.2 kDa, Mw of cellulose monomer = 162.14 g mol^{-1}. [b] Diazirine is theoretically grafted on 20% of the 128 amine end groups of PAMAM, 1 mol of PDz will have [diazirine] = (0.20 × 128) = 25. [OH] depends on the cellulose, 1 mol of cellulose will have [OH] = 6. Assuming 100% Dz is crosslinked, at theoretical 20% Dz grafting on dendrimer, 1 mol PDz will bind 4 mole cellulose. [c] $G' < G''$ – viscous, $G' > G''$ – Bingham plastic in uncured state.

Table 2 Material properties of BC_PDz(h) formulations before and after curing at varying %BC

Total solute % (w/w)	PDz w/w% (mM)	BC w/w% (mM)	[Diazirine]/[OH] mol ratio	G' before curing (kPa)	G' max at UV off (kPa)	Gelation UV dose (J)	Uncured state
20	20.0 (6.8)	0.0 (0.0)	—	<0.001	<0.001	No gelation	Viscous
20	19.7 (6.8)	0.3 (20)	1.4	0.1 ± 0.1	0.9 ± 0.3	4.3 ± 0.8	Viscous
20	19.5 (6.8)	0.5 (40)	0.7	0.8 ± 0.5	2.3 ± 0.2	3.5 ± 0.7	Viscous
20	19.0 (6.8)	1.0 (80)	0.35	1.7 ± 0.3	3.2 ± 0.5	2.6 ± 0.7	Bingham plastic
33.3	33.3 (13.6)	0.0 (0.0)	—	<0.001	1.4 ± 0.3	7.2 ± 0.3	Viscous
33.3	33.0 (13.6)	0.3 (20)	2.8	0.9 ± 0.2	6.2 ± 1.0	8.2 ± 1.1	Viscous
33.3	32.8 (13.6)	0.5 (40)	1.4	1.3 ± 0.8	5.0 ± 0.6	5.2 ± 0.4	Viscous
33.3	32.3 (13.6)	1.0 (80)	0.7	3.3 ± 1.1	8.9 ± 2.1	2.3 ± 0.8	Viscous

uniform mixing. The obtained BC_PDz(h) formulations were then employed for further experiments.

Real-time photorheometry evaluation of BC_PDz(h) composites. Rheometry measurements were conducted with Anton Paar Physica MCR 102 rheometer fitted with parallel plate probe PP10 and UVA transparent glass slide, as presented in Fig. 2A. The applied UVA intensity (365 nm) was calibrated to 100 mW cm^{-2} with an IL 1400 Radiometer using a 365 nm LED setup (SOLIS-365C, THORLABS) with current input of 1300 mA. The parameters of dynamic oscillatory strain were set as follows: 0.45 mm measuring gap, 1% amplitude, and 10 Hz frequency. The storage modulus (G') and loss modulus (G'') were evaluated in the first 30 s to determine dynamic viscosity (phase I), followed by photocuring using UVA irradiation for 100 s (phase II), and an amplitude sweep of 1–1000% at 1 Hz (phase III) as presented in Fig. S1A in ESI.†

SEM imaging. BC_PDz(h) composites were placed between PET films and photocured with UVA dose of 10 J cm^{-2} (365 nm, 100 mW cm^{-2}). After photocuring, the PET sheets were peeled apart to expose the cohesively fractured composite matrix which was subsequently analyzed for structural morphology. A field emission scanning electron microscope (JEOL, JSM-6700 F, Japan) (accelerating voltage of 5 kV and 8 mm working distance) was employed to observe the structural morphology of the cured BC_PDz(h) composites. The samples were sputter coated (JEOL JFC-1600 Auto Fine Coater) with platinum for 70 s, 20 mA current in vacuum (8–9 Pa) before imaging. ImageJ[36] software was employed to determine the pore length and pore number per unit area as per the method previously described in Shah *et al.*[37] The scale bar was utilized as a measurement reference, and the longest length on the pore is recorded.

Lap shear adhesion assessment against PLGA and wet tissue mimics. PLGA films (2 × 1.5 cm^2) and hydrated collagen films as wet tissue mimics (2 × 1.5 cm^2)[38] were fixed on the glass slides using double sided adhesive tape. BC_PDz(h) composites (10 mg, 100 μm thickness) were then smeared in between the films and activated by UVA (365 nm, 100 mW cm^{-2}) for 100 seconds (10 J UV dose). The adhesion strength of the formulated BC_PDz(h) composites was determined using modified tensile tester (Chatillon force measurement, Largo, FL, USA) with a controlled linear speed of 3 mm min^{-1} with 50 N load cell (n = 5).[23]

Statistical analysis. All data were presented as mean ± SD (n = 3, unless otherwise stated). OriginPro 2018 64-bit software was employed to determine significance using two-way ANOVA with Bonferroni as *posthoc* test. A $p < 0.05$ (*) was considered statistically significant. Rheology and lap shear adhesion curves were smoothed to remove transient noise by using percentile filter and Loess (span 0.1) method, respectively.

Results

Formulation and design of BC_PDz(h) hydrogels

Layered film composites of BC and PDz (BC_PDz(lc)) were found to have extended structural integrity in aqueous shear environments *ex vivo* for 7 days.[19] To extend the applicability of these systems for irregularly shaped surfaces, liquid or low yielding Bingham Plastic BC_PDz(h) bioadhesives are sought. Formulation of viscous or low yielding precursors from BC requires chemical or mechanical structure disintegration.[39] Fig. 1 illustrates the stepwise procedure for BC_PDz(h) formulation starting with BC pellicle. Sonication is chosen to

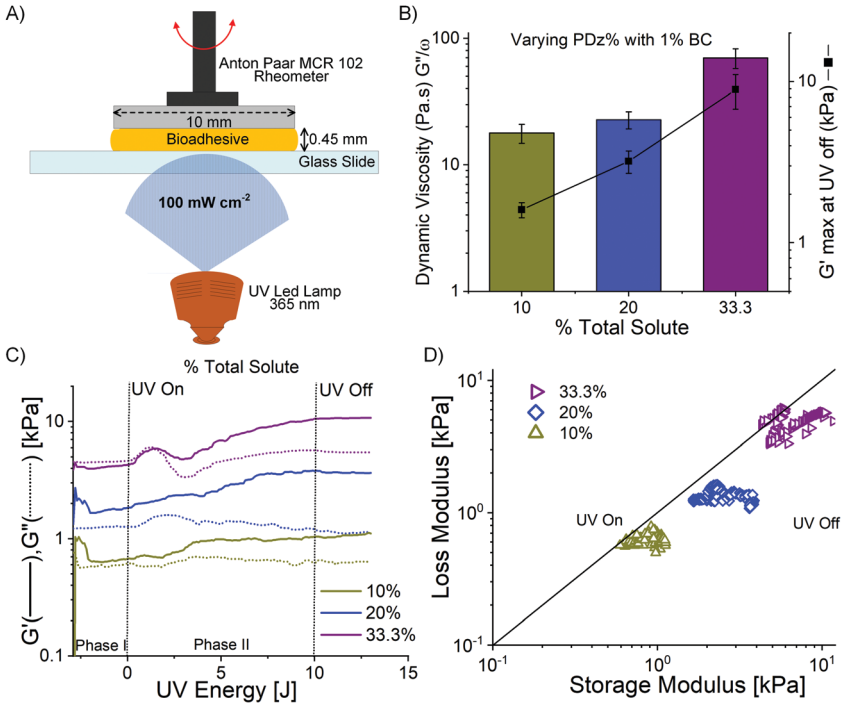

Fig. 2 (A) Schematic representation of photorheology setup with glass slide as sample holder and probe, equipped with UV source; (B) dynamic viscosity of pre-crosslinked formulations (bar graph); comparative results of G' maximum measured at UV energy of 10 J (scatter); (C) representative photorheometry diagrams of dynamic change of G' and G'' during UV exposure in the range of 0–10 J; (D) BC_PDz(h) vector plots (gelation line) representing G^* (complex modulus) within the UV curing energy range of 0–10 J. The formulations consist of 1% BC and varying %PDz. Data presented as mean ± SD, n = 3.

fibrillate the BC matrix as it avoids chemical treatment and its risk of trace leachates. Aqueous adhesive composites are formulated by mixing varying percentages of BC and PDz (Tables 1 and 2). BC exhibits concentration dependent viscosity. For concentrations below 0.5%, BC behaves as liquid while for any weight% higher than 0.5%, it turns into a Bingham plastic (pseudoplastic solid with a low yield stress, Fig. S2B–D, ESI†). Consequently, the BC_PDz(h) is formulated between 0.3% and 1% BC. The binary composites are evaluated for real-time mechanical properties through a customized photorheology setup (Fig. 2A). The three-phase rheology protocol (viscosity, complex modulus, strain) evaluates the liquid to solid transition with respect to Joules cm^{-2} light exposure (Fig. S1A, ESI†). Structure–activity relationships of solute weight%, macromer mole ratio are correlated to gelation time/dose, material properties and adhesion strength of the composites. Rheological properties (dynamic viscosity, loss modulus (G'')/storage modulus (G'), and yield stress/strain) are determined with respect to total solute percentage and UVA dose. Porosity of the photocured bioadhesives is analyzed by electron microscopy of the surfaces. Lap shear adhesion assesses the cohesive strength and viscoelastic dissipation when applied to natural and synthetic substrates.

Composites allow a 2.5 fold reduction of PDz while retaining viscous liquid to solid gelation

The BC native pellicle is sonicated to obtain a final concentration of 1.3 ± 0.2% w/w. The hydrogel concentration is limited by the cellulose weight synthesized by *G. hansenii* bacteria upon 5 days of incubation. The BC hydrogel (1.3% w/w) is further used for formulating the composites, resulting in final concentrations of 0.3–1% w/w BC in the composites (Tables 1 and 2). In the previous BC film-based platform, the concentration of PDz bioadhesive was 50%. However, lower concentrations of PDz is desired to reduce tissue exposure of cationic $-NH_2$ groups and the associated cytotoxicity.[28,29] Thus, lower concentrations of PDz (9–32.5%) are evaluated in the present compositions. Composites with total solute (solute %BC + solute %PDz) lower than 10% did not achieve gelation ($G' \geq G''$) after 10 J UVA exposure, therefore dropped from the study. The primary aim of this experiment is to minimize the weight% (wt%) of PDz (active crosslinker), while achieving light activated gelation. BC wt% should be as high as possible while retaining a viscous formulation ($G'' \geq G'$) or a spreadable pseudoplastic solid before light curing. A spreadable solid (Bingham Plastic) requires a yield stress before viscous deformation. The total solute percentage of aqueous adhesives is thus varied from 10% to 33.3% (PDz of 9–32.5% + BC) which further leads to varying BC, PDz moles and [Diazirine]/[OH] mole ratio (Table 1). Real-time photorheology determines the degree of UVA dependent cross-linking. The corresponding changes in the storage modulus (G') and loss (G'') modulus are recorded with respect to %w/w solute as shown in Fig. 2 and summarized in Table 1. During Phase I (UVA off), a 1% oscillatory strain disrupts weak intermolecular attractive forces, and dynamic viscosity is evaluated over a 30 s time period. Total solute percentage correlates to viscosity from 18 to 70 Pa s (Fig. 2B, Pearson's r = 0.94). Phase II (UVA on) evaluates G' and G'', 0 to 10 J (Fig. S1A, ESI†). G'

value measured at 10 J UVA dose ranges from 1.6 kPa to 8.9 kPa with 10–33.3% total solute percentage (Pearson's r = 0.97) as presented in Fig. 2B. The representative photocuring profiles of BC_PDz(h) composites are observed in Fig. 2C. This is the first observation of gelation at PDz at 10% and 20%. Prior investigations required a minimum of 25% G5-*g*-diazirine solute to achieve gelation in saline solutions.[24,25,37,40,41] The photocuring kinetics of BC_PDz(h) composites from Fig. 2C are replotted as a vector plot to visually compare viscoelastic properties in Fig. 2D. A diagonal line marks the gelation point, defined as $G'' = G'$ or $\tan\delta = 1$. The line also divides the plot into two regions, the viscous region (above the line) and solid-like regions (below the line). BC_PDz(h) composites at 1% are expected to behave as hydrogels with solid-like material properties as seen with 10% and 20% total solutes. Only the 33.3% total solute composites observes viscous liquid to solid-like transition under UVA exposure. This suggests that the globular PDz acts as a lubricant, separating the BC chains from forming weak interactions. Composites with 20% and 33.3% total solute are studied further for effects of %BC, %PDz and [Diazirine]/[OH] mole ratios on material properties (Table 2). Owing to relatively low storage modulus (1.6 ± 0.2 kPa) approaching the maximum concentration of BC, composites with 10% total solute are not evaluated further.

Diazirine/OH mole ratios of near one have the biggest shifts in complex modulus G^*

PDz to BC mole ratios' effect on dynamic material properties are evaluated with fixed 20% and 33.3% total solute composites (PDz is slightly lowered as BC varies) as shown in Table 2. %BC are varied from 0.3–1%. Fig. 3A represents the dynamic viscosity of the formulations in Phase I of photorheology. The dynamic viscosity ranges from 4 to 22 Pa s for 20% total solute composites and 45–100 Pa s for 33.3% total solute. Formulation with 20% total solute, 1% BC (Fig. 3C) is Bingham plastic ($G' > G''$ before photocuring), whose low yield stress allow shaping before application. All other composites are viscous in nature ($G' < G''$ before photocuring) (Fig. 3C and D). The increase in %BC is positively correlated (Pearson's r = 0.89) with the increase in dynamic viscosity for 20% total solute composites. Maximum G' value measured at 10 J UVA dose is presented in Fig. 3B. Increase in %BC leads to an increase in G' for both groups (0.6–3.7 kPa for 20% (Pearson's r = 0.97), 1–11 kPa for 33% (Pearson's r = 0.89). Moreover, an increase in the total solute percentage leads to a significant increase in maximum G' for all the corresponding BC percentages. The G' before photocuring (Table 2) for the composites increase with increasing %BC (Fig. S2B, ESI†). However, upon photocuring, the composites exhibit 2–9 times rise in the G' (Table 2). The representative photocuring profiles of BC_PDz(h) composites with varying %BC (0.3%, 0.5% and 1%) are presented in Fig. 3C and D for 20 and 33.3% total solute respectively. It can be observed from Fig. 3C that composites with 0.3% and 0.5% BC exhibit viscoelastic liquid to solid transition as photocuring progresses (UV dose 3.5–4.3 J, 35–40 seconds, Table 2). Increase in %BC also leads to reduced UV dose required for crosslinking (Table 2).

In case of 33.3% total solute photorheograms presented in Fig. 3D, all composites start off as viscoelastic liquid then changing to viscoelastic solid upon photocuring (2.3–8 J, 23–80 seconds). UV Joules required to crosslink the composite are reduced as the %BC increase (2.3 J for 1% BC, 33.3% total solute compared to 7.2 J for 0% BC, Table 2). The composites with varying BC percentages exhibit G' values 3–5 times higher than that of 33.3% PDz with 0% BC, suggesting BC addition increases the storage modulus upon crosslinking. The photocuring kinetics of BC_PDz(h) composites from Fig. 3C and D are replotted as a vector plot to evaluate the changes in the viscoelastic properties of the composites during curing in Fig. 3E and F. It is observed that the BC_PDz(h) composites progress from the liquid region and as the curing continues transition into solid-like material properties with elastic modulus values in kPa range for 0.3% and 0.5% BC in both groups and 1% BC in 33.3% total solute group. In contrary, composites with 1% BC in 20% total solute are pseudoplastic before curing and exhibit a rise in the elastic modulus upon photocuring. None of the controls (varying %BC Fig. S2C and BC_PAMAM Fig. S3C, D, ESI†) exhibited any change in the G', G'' upon photocuring. Fig. 3G and H represent the %change in complex modulus G^* before (0 J) and after (10 J) photocuring for varying total %solute and %BC respectively (%shift in $G^* = \left(G^*_{10\,\mathrm{J}} - G^*_{0\,\mathrm{J}}\right) \times 100/G^*_{0\,\mathrm{J}}$). Increasing %total solute (%PDz) does not exhibit significant change in G^* (Fig. 3G). However, composites with Diazirine/OH mol ratios of near one (20%, 0.3% BC & 33.3%, 0.5% BC, Table 2) exhibit significantly higher increase in the complex modulus upon photocuring (Fig. 3H). Overall the composites exhibit about 20–300 times increase in G^* for varying %solute and %BC.

BC controls material properties while PDz acts as plasticizer

The third phase of photorheology consists of amplitude sweeps ranging from 1–1000% strain performed after photocuring as depicted in Fig. S1A (ESI†). The amplitude sweep helps to determine the linear viscoelastic range (LVR), yield point (yield stress and strain), as presented in Fig. 4. Cured BC_PDz(h) composites have no clear LVR-a non-linear modulus is observed in Fig. 4A and B. Stress at yield point ($G' = G''$) exhibits a strong correlation with total solute percentage for BC_PDz(h) composites (Pearson's r = 0.99), as presented in Fig. 4C. The variation of $\tan\delta$ with shear strain for the composites is presented in Fig. 4D. It is observed that composites with 1% BC for both groups exhibit an increase in $\tan\delta$ starting from as low as 2% strain. All other composites exhibit increasing $\tan\delta$ values starting from 40% strain. Thus, the results suggest that the initial viscosity, loss modulus, and post-curing yield stress composites can be tuned based on %BC.

Inclusion of BC in the composite reduces pore frequency

Surface morphology of cohesively fractured adhesive composites is imaged to evaluate the variation in pore length and pore number due to BC and PDz concentrations. No pores are observed in the case of photocured 20% PDz (Fig. 5A), which

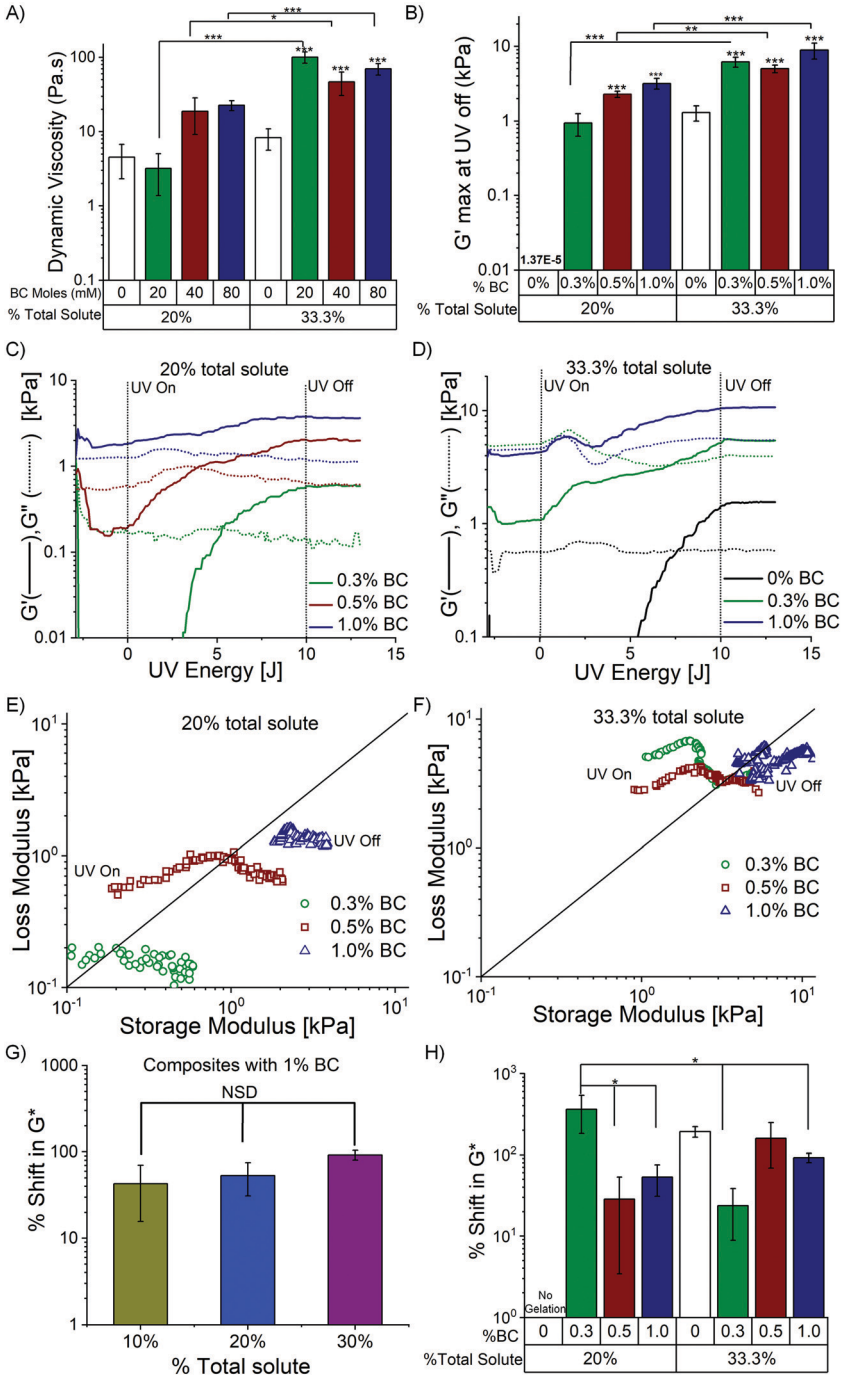

Fig. 3 Rheological properties of BC_PDz(h) composites with varying BC moles in the composites with total solute percentage fixed at 20% and 33.3%. (A) dynamic viscosity of pre-crosslinked formulations; (B) comparative results of G' maximum measured at UV energy of 10 J; representative photorheometry diagrams of dynamic change of G' and G'' during UV exposure in the range of 0–10 J; (C) 20% total solute (0% BC composite did not crosslink after 10 J); (D) 33.3% total solute (photorheograms for 0.3% and 0.5% BC composites are overlapping); BC_PDz(h) vector plots (gelation line) representing G^* (complex modulus) within the UV curing energy range of 0–10 J; (E) 20% total solute; (F) 33.3% total solute; comparative % shift in the complex shear modulus G^* upon photocuring for (G) varying % total solute; (H) varying %BC for 20%, 33.3% composites. %Shift in $G^* = \left(G^*_{10\,\mathrm{J}} - G^*_{0\,\mathrm{J}}\right) \times 100/G^*_{0\,\mathrm{J}}$. Data presented as mean ± SD, n = 3, p-values are calculated using two-way ANOVA with Bonferroni *post hoc* test, *$p < 0.05$, **$p < 0.01$, ***$p < 0.001$. (In (H), one outlier has not been included in analysis for 20% total solute_0.5% BC composite.)

indicates that the formulation is reflowing. However, composites with 20% total solute (Fig. 5B and C) exhibit pores of 100–300 μm size (Fig. 5G, similar to photocured BC_PDz(lc) films Fig. 5I [19]), with pore count exhibiting a negative correlation (Pearson's $r = -0.77$) with increasing %BC. The 33.3% PDz formulation (Fig. 5D) exhibits uniform pore distribution over

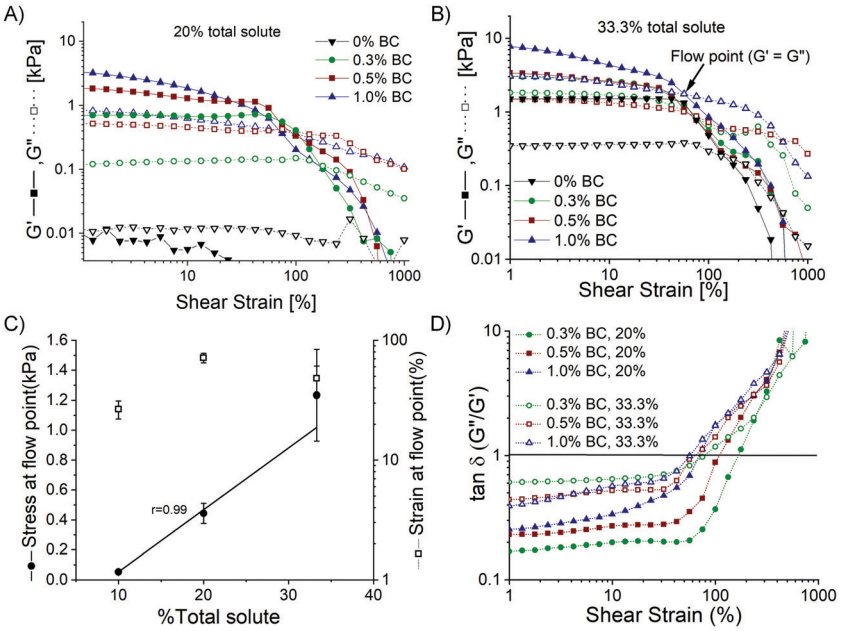

Fig. 4 Amplitude sweep of crosslinked BC_PDz(h) composites after photocuring for composites of varying %BC with (A) 20% total solute; (B) 33.3% total solute; (C) stress and strain at flow point ($G' = G''$) plotted with Pearson's r values for composites of varying total solute percentage; (D) variation of tan δ (G''/G') with shear strain for composites of 20 and 33.3% total solute percentage. Data presented as mean ± SD, n = 3.

the area suggesting that it is cured and forms a porous matrix. Similarly, 33.3% composites (Fig. 5E and F) exhibit uniform pores of 10–80 μm size independent of %BC (Fig. 5H, lower pore size, higher pore count than photocured BC_PDz(lc) films Fig. 5I[19]) and positive correlation (Pearson's r = 0.99) of pore count with increasing %BC (Fig. 5H, lower pore count compared to 0% BC). The composites exhibit a decrease in the pore size and increase in the pore count as the total solute increases from 20% to 33.3%. This can be attributed to the increased PDz amount available to react.

Tunable adhesion is observed on both synthetic and natural materials

A lap shear test is performed to determine the maximum adhesion strength exhibited by the composites against

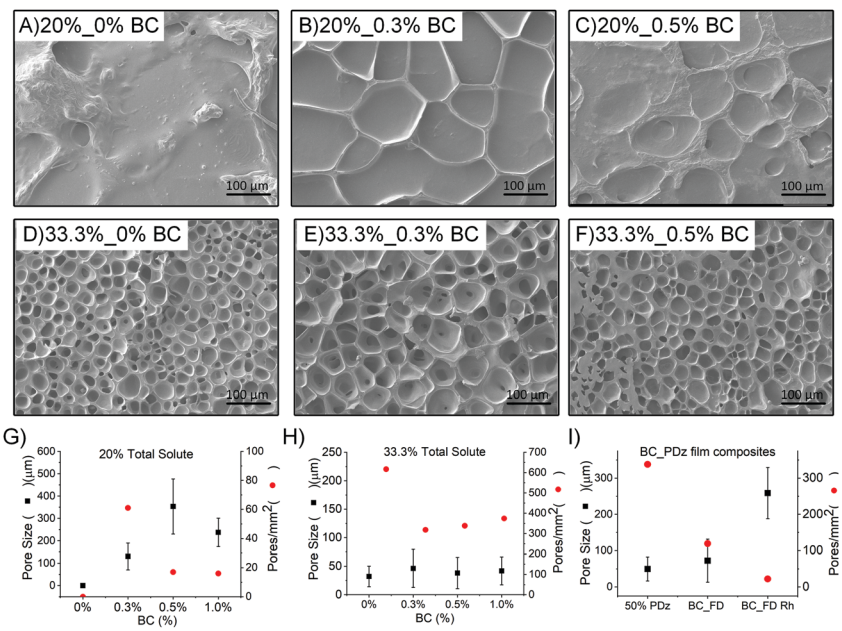

Fig. 5 SEM images of cohesively fractured photocured BC_PDz(h) composite surface of 20% total solute (A–C), BC ranging from 0–0.5%; composites with 33.3% total solute (D–F), BC ranging from 0–0.5%; Average pore size, count for the cured BC_PDz(h) composites with varying % BC and (G) 20% total solute; (H) 33.3% total solute; (I) BC_PDz(lc) film composites.[19] The composite name is defined as %total solute_%BC.

hydrophilic (wet tissue mimic, hydrated collagen) and hydrophobic substrates (PLGA). Fig. 6A illustrates the experimental setup of the lap shear test of photocured BC_PDz(h) composites against substrates. The composites placed in the sandwich structure are exposed to UVA (365 nm, 100 mW cm^{-2}, 10 J UV dose). The representative stress–strain profiles obtained by lap shear test with PLGA films is presented in Fig. 6B and C for 20% and 33.3% total solute, respectively, and Fig. 6D compares the maximum adhesion strength at failure. Composites with 20% and 33.3% total solute exhibit mean adhesion strength ranging from 8–40 kPa to 22–70 kPa, respectively, for varying %BC. Composites with 20% total solute exhibit negative correlation with increasing %BC and decreasing [Diazirine]/[OH] ratio (Table 2, Pearson's $r = -0.87$). Increasing %PDz in composites with 0.5% and 1% BC leads to significantly higher adhesion strength (***$p < 0.001$ and *$p < 0.05$ respectively). The highest adhesion strength is exhibited by 0.3% BC, 20% solute and 0.5% BC, 33.3% solute in their respective groups. Interestingly both formulations exhibit viscous to elastic solid transition upon gelation and have [Diazirine]/[OH] mole ratio of 1.4, while also exhibiting the highest shifts in G^* upon photocuring (Fig. 3H). This suggests that addition of BC to composites leads to increased adhesion strength through a tougher cohesive matrix. An increase of PDz crosslinker does not always lead to better adhesion strength—other viscoelastic factors appear to influence the overall adhesion strength. The bioadhesives are then evaluated against a hydrophilic wet substrate.

Fig. 7A and B depict representative stress–strain curves for 20% and 33.3% BC_PDz(h) composites performed against wet tissue mimic (following previously reported protocol[38]) with Fig. 7C comparing the maximum adhesion strength at failure. Composites with 20% and 33.3% total solute exhibit mean adhesion strength of 3–33 kPa and 8–30 kPa, respectively. Composites with 20% solute with 0.5% BC and 33.3% solute with 0.3% and 1% BC exhibit significantly higher adhesion strength compared to respective controls. All these composites exhibit viscous to elastic solid transition undergoing gelation and have higher [diazirine]/[OH] mole ratios (0.7–2.8 Table 2). Moreover, increase in %PDz for composites with 0.3% and 1% BC leads to significant increase in adhesion strength (*$p < 0.05$ and *$p < 0.05$, respectively). The high standard deviation can be attributed to factors like variations in the hydration extent of the wet tissue mimic.

Overall, the composites exhibit adhesion strength with a range of 8–70 kPa against synthetic PLGA substrates and 3–35 kPa against wet tissue mimic. The adhesion strength is lower in the case of wet tissue mimics which is expected due to carbene fouling with water.[23,42,43] Fig. 7D represents the comparison of maximum adhesion strength of BC_PDz(h) and BC_PDz(lc) film based adhesive systems with varying UV dose, BC percentage and total solute percentage. It is observed that the aqueous hydrogel systems exhibit similar adhesion strength to that of the previously reported adhesive BC_PDz(lc) film systems[19] (not significantly different $p > 0.5$). Moreover, the adhesion strength can be tuned

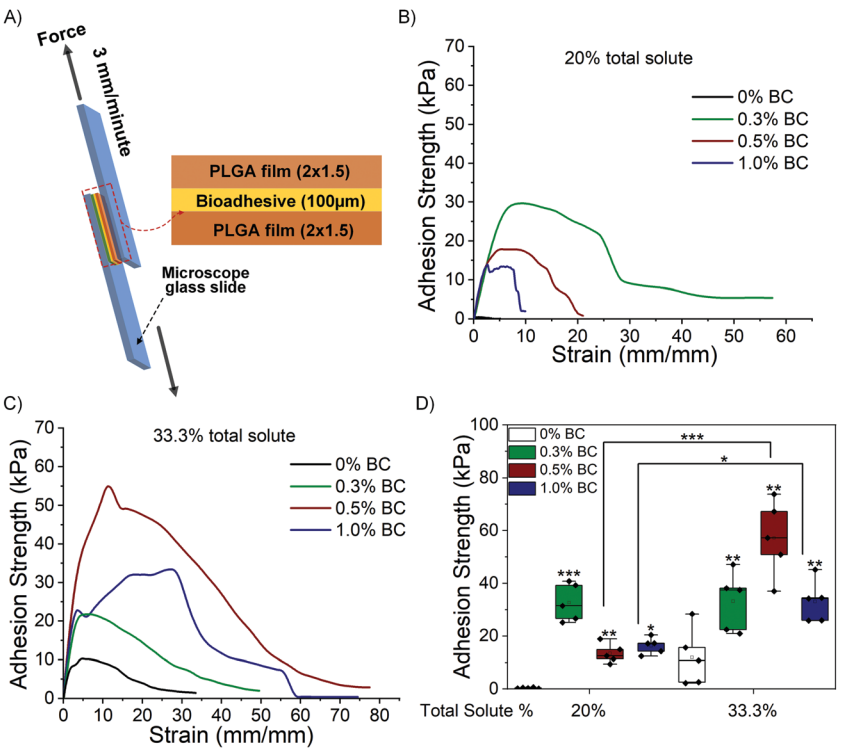

Fig. 6 Lap shear adhesion dependence on total solute percentage and %BC. (A) Illustration of the sandwich setup for lap shear test consisting of PLGA films and BC_PDz(h) bioadhesive; representative adhesion strength *versus* strain curves performed against PLGA for varying %BC composites with (B) 20% total solute; (C) 33.3% total solute; (D) Maximum adhesion strength at failure for composites with varying total solute percentage and %BC. Data presented as mean ± SD, $n = 5$, p-values are calculated using two-way ANOVA with Bonferroni *post hoc* test, *$p < 0.05$, **$p < 0.01$, ***$p < 0.001$.

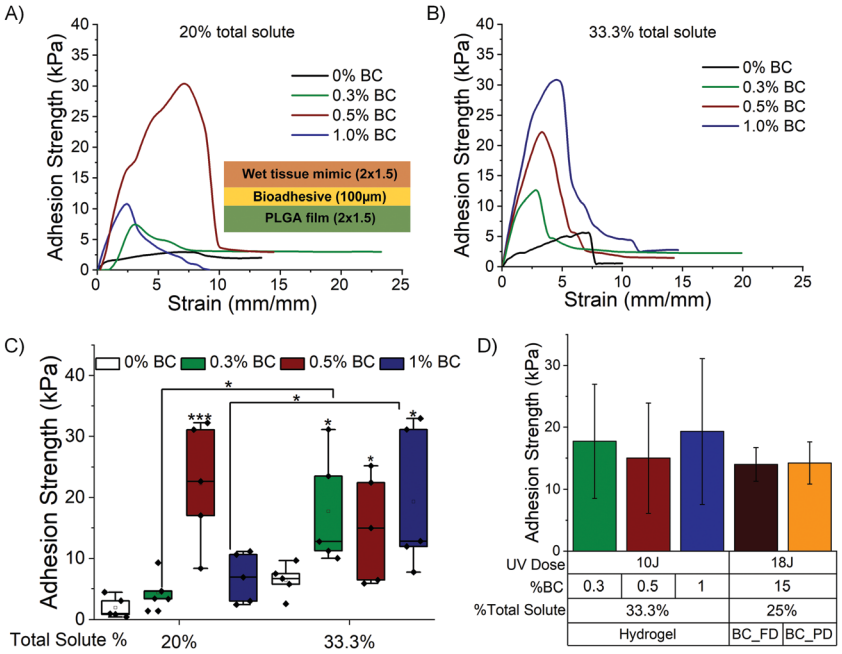

Fig. 7 Representative adhesion strength *versus* strain curves performed against wet tissue mimic for varying %BC composites with (A) 20% total solute; (B) 33.3% total solute; (C) maximum adhesion strength at failure for composites with varying total solute percentage and %BC. (D) Comparison of adhesion strength of BC_PDz(h) systems with that of BC_PDz(lc) film-based systems. Data presented as mean ± SD, $n = 5$, p-values are calculated using two-way ANOVA with Bonferroni *post hoc* test, $*p < 0.05$, $**p < 0.01$, $***p < 0.001$.

by modulating the concentrations of BC and PDz in the composites. Composites with higher [diazirine]/[OH] mol ratios (1.4–2.8) exhibit the highest adhesion properties to both dry and wet substrates. The maximum adhesion strength exhibited by the hydrogel systems against wet surfaces is similar to previously reported synthetic PDz composites dissolved in PEG solvents (5–25 kPa).[24,37,40] The systems exhibit higher adhesion strength compared to mucoadhesive systems (8–50 Pa)[11,44–46] and lower than mussel inspired adhesive systems (5–160 kPa).[16–18,47,48]

Discussion

Existing topical mucoadhesives for oral applications require 6–10 minutes curing time and harsh chemical agents (silver nitrate, sodium periodate, glutaraldehyde), while exhibiting low storage modulus (G' 0.01–0.1 kPa) and low adhesion strength against wet substrates (0.5–5 kPa). These limitations lead to the need for frequent applications and reduced patient compliance. Thus, there exists a clinical need for mucoadhesives that conform to complex surfaces and tight spaces, *e.g.* gingiva, hard plate, tonsils, and mouth floor. In this study, viscous and malleable mucoadhesives were synthesized from fibrillated bacterial cellulose (BC) and light-activated bioadhesives dendrimer (PDz). BC hydrogel was hypothesized to control the rheological properties while PDz (G5-PAMAM grafted with diazirine), the adhesion to wet surfaces. The composites exhibit tunable dynamic viscosity (18 to 70 Pa s) and the capability of viscous liquid (free flowing) or malleable Bingham Plastic (mayonnaise consistency, η = 20 Pa s) formulations. Both can be applied to irregular surfaces, but Bingham plastics have the advantage of retaining their shape while photocuring. Shear moduli ranges from 1–10 kPa, which mimics that of soft palate[49] and other oral mucosal tissues.[50–52]

BC is most commonly synthesized by aerobic bacteria *Acetobacteraceae* family members.[53] Unlike plant derived cellulose, BC consists of a nanofibrous matrix (BC dispersion, Fig. S5, ESI†). The complex molecular structure is a result of hydrogen bonding with inter and intra-molecular glucan chains and bound water.[54] The presence of hydrogen bonds in the wet BC matrix provides it with a rigid structure on molecular level and mechanical flexibility.[30] BC can be fibrillated and formed into hydrogel with viscosity (η_{app} = 0.4–10 Pa s) that correlates to %BC (0.2–1%) (Fig. S2A, ESI†). Hydrogels with %BC greater than 0.5% behave as Bingham Plastic while that lower than 0.5% behave as viscous formulations (pseudoplastic fluid, Fig. S2B, ESI†). This property of BC to form viscous liquid/Bingham Plastic is utilized herein to formulate malleable mucoadhesives in combination with PDz. Mixing with PDz changes the rheological properties where BC_PDz(h) composite with 1% BC behaves as Bingham Plastic while all other formulations are viscous liquid (Fig. 2C, D, 3C–F, and Tables 1, 2). BC's rheological nature is unaffected when it is mixed with neat G5-PAMAM (Fig. S2E, F, S3B–D, ESI†). Thus, the loss of $-NH_2$ or the presence of diazirine groups of PDz appears to disrupt the weak attractive forces between BC chains. The combination of BC with PDz (20%) makes possible the viscous liquid to solid gelation, which is not possible for either component alone (Fig. 3B and Fig. S1C, S2C, D, S3C, D, S4, ESI†). Composites with total solute lower than 10% were dropped from the study

as they did not exhibit gelation ($G' > G''$ not present after photocuring) as opposed to 10–33.3% solute composites. Gelation is the transition point where viscous liquid formulations solidify into viscoelastic films upon photocuring, thus preventing wash-off/erosion. Addition of varying %BC into PDz offers formulations with yield stress varying from 1–50 Pa (Table S1, ESI†). The yield stress increases about 10–400 times for 20% composite photocured formulations and 50–2400 times for 33.3% composites (Table S1, ESI†). The initial yield stress for 20 and 33.3% BC_PAMAM formulations are similar, however photocured BC_PDz(h) formulations exhibit 2–4 times higher yield stress as %total solute increases (Table S1, ESI†). Higher concentration of PDz leads to higher adhesion strength alongwith higher pore count (Fig. 5) formed due to the nitrogen molecules released upon carbene formation as reported earlier.[33,37,41] Uniform distribution of pores assert homogenous mixing of PDz and BC in the photocured hydrogel. Cohesive fracture through the matrix upon peeling away of PET sheets for pore analysis assures no tissue damage upon removal.

PDz, the second component exhibits shear moduli and adhesion strength variable with the percentage of diazirine conjugation, the concentration of the PDz and UV dose.[55] For the PDz (20% conjugation), the lowest concentration evaluated was 25% which upon photocuring exhibited storage modulus (G') of 1–3 kPa and adhesion strength (AS) of 5 kPa against wet tissue. Shear moduli (20–200 kPa) and adhesion strength (25–35 kPa) increased with the increased PDz concentration (50, 75%).[55] However, PDz exhibits limitations such as foaming caused by the nitrogen release, non-specific reaction with water molecules (causing trade-off between adhesion strength and pore formation), and cationic $-NH_2$ groups exposure to mammalian tissues. Thus, lower concentration of PDz is desired to reduce cationic $-NH_2$ groups and the associated cytotoxicity.[28,29] Attempts to overcome these limitations involve replacement of the aqueous solvent of PDz by hydrophilic PEG 400[37] (G' 25 kPa, AS 5–10 kPa) or hydrophobic polycaprolactone triol (PCLT, G' 0.1–4 kPa, AS 5–25 kPa).[24] Table 3 compares the material properties of current BC_PDz(h) formulation to other PDz composites. PEG_PDz overcomes the limitation of non-specific reaction with interfacial water layer due to hygroscopic nature of PEG and higher PDz concentrations. However, the formulations exhibit swelling (400% by mass), burst release of PEG and cannot be dried into powders.[37] PCLT_PDz is expected to exhibit low swelling as PAMAM/polycaprolactone composites have been reported to swell about 30% in saline.[24,56] However, PCLT molecules have no shelf stability with PDz owing to accelerated ester hydrolysis in amine environment.[57] PDz composites with platelet-rich plasma (PRP) have been evaluated to improve the biocompatibility (G' 80–120 kPa, AS 10–20 kPa).[27] However, the increased biocompatibility comes as a tradeoff in shelf stability, as all PRP formulations would need to be freshly prepared at the point of application.[27] Comparable to this study was the PDz composite with 350 kDa alginate which exhibited G' of 30 kPa and adhesion strength of 8–10 kPa against wet substrates.[40] Early attempts of mixing biopolymers, such as alginate, with PDz exhibited electrostatic crosslinking, resulting in Bingham Plastics with shear moduli approaching 1 MPa – too stiff for bioadhesives applications.[58] On the other hand, BC provides hydrogel structures without electrostatic interactions (Fig. S3 and Table S1, ESI†) and shear moduli comparable to soft tissues. The study with PEG_PDz also suggested negative correlation between effective G' after photocuring and the initial measuring gap.[37] Taking in consideration previous studies with shear moduli, the BC_PDz(h) aqueous composites exhibit comparable shear moduli to non-aqueous PCLT_PDz and PEG_PDz composites even when prepared at 4× the thickness. BC_PDz(h) composites are demonstrated to exhibit adhesion to synthetic, hydrophobic substrates (20% PDz – 40 kPa AS, 33.3% PDz – 70 kPa AS, 2–3 times higher than PCLT_PDz composites) as well as natural, hydrophilic substrates (20% PDz-33 kPa, 33.3% PDz-30 kPa, 2–3 times higher than PEG_PDz, PCLT_PDz and alginate_PDz[40] composites). The BC_PDz(h) composites also allow reduction of total solute% to as low as 20%. Aqueous BC_PDz(h) exhibits adhesion strength similar to previously reported adhesive BC_PDz(lc) film systems (Fig. 7D). Layered BC_PDz(lc) film composites yielded moderate adhesion strength 7–17 kPa that withstood days of aqueous shear strain owing to combination of PDz-mediated covalent bonding and BC's hydration-resistant cohesive strength.[19] The layered film composites can thus be used as platform towards mucoadhesive delivery systems wherein prolonged adhesion and structural integrity is desired at regularly-shaped disease sites. However, for irregularly-shaped surfaces, liquid or low yielding Bingham Plastic BC_PDz(h) bioadhesives are preferred as it can be easily spread to the disease site followed by viscous liquid to elastic solid transition upon photocuring. BC_PDz(h) with the following compositions (%total solute_%BC): (1) 20%_0.5% BC and (2) 33%_0.3% BC are best for application as mucoadhesives owing to optimal material properties (gelation dose – 3.5–8.2 J, gelation time – 35–80 s,

Table 3 Comparison of material properties of PDz composites with various biopolymers

			Lap shear adhesion strength (kPa)				
Biopolymer	%PDz	%total solute	Tissue	Dry substrate	G' storage modulus (kPa)	Gelation UV dose (J cm^{-2})	
BC (this study)	19–32.9	20–33.3	3–33	8–70	1–10	2–8	Aqueous
PDz[23]	25	25	25–35	—	20–200	1–6	Aqueous
PRP[27]	50	—	10–20	—	80–120	2	Aqueous
PEG[37]	30	100	5–10	—	25	3–5	Non-aqueous
PCLT[24]	20–33.3	100	5–25	1–15	0.1–4	6–10	Non-aqueous
Alginate[40]	—	—	8–10	—	30	4–5	Aqueous

G' max – 2–7 kPa) and the highest shear adhesion strength against wet tissue mimic.

Existing mucoadhesives exploit hydrogen bond interactions as the adhesion mechanism, resulting in low adhesion strength (8–50 Pa) and low storage modulus (0.01–0.1 kPa). Adhesion strengths of mucoadhesive systems have been reported to be 8–16 Pa (assuming area of 3 cm^2) for chitosan, hydroxypropylmethylcellulose (HPMC), and xanthan gum films (G' 0.01–100 Pa),[11] 33 Pa (assuming area of 3 cm^2) for xanthan gum based emulsion,[45] 50 Pa (assuming area of 3 cm^2) for adhesive system composed of eudragits (a mixture of methyl and ethyl acrylates), and HPMC[44] and 60–200 Pa (assuming area of 3 cm^2) for hydrogels composed of hyaluronic acid, xanthan gum, carboxymethylcellulose, hydroxyethylcellulose, alginate, Carbopol® and polycarbophil (G' 0.1–1 kPa).[46] The lap shear tests exhibit about 2–5 times higher adhesive strength than normal/tensile test.[59] Taking that into consideration, the average adhesion strength for these mucoadhesives relying on hydrogen bonds ranges from 0.5–5 kPa. BC_PDz(h) composites exhibit higher adhesion strength of 3–35 kPa which can be attributed to the covalent bond mechanism by carbene insertion, electrostatic interactions ($-NH_2$ groups PDz with acid moieties in the oral mucosal layer[60]) and mechanical interlocking of BC nanofibers with the mucosal proteins mechanisms.[61] An increase in ester group absorbance upon photocuring is observed which can be due to the reaction of carbene with –OH groups and increase in –C–C– bonds due to reaction of carbene with $-CH_2$ groups as hypothesized in Fig. 1 (ESI,† Fig. S6 and Table S2). Apart from drug-loaded mucoadhesive system, mussel inspired bioadhesive systems have been evaluated. Guo *et al.*[17] reported wet adhesion through tannic acid-based bioadhesives exhibiting adhesion strength of 30–50 kPa, G' of 10 Pa, and minimum gelation time of 240 seconds requiring addition of silver nitrate solution. Another citrate-based mussel inspired bioadhesive crosslinked upon addition of oxidative silver nitrate and sodium periodate exhibited adhesive strength of 30–160 kPa and high gelation time of 60–500 seconds.[18] Nutan *et al.*[16] reported prepolymer liquid-based system which transformed into *in situ* bioadhesive amphiphilic systems (gelation upon addition of poly(2-dimethylaminoethyl)methacrylate (PDMA) to prepolymer mixture of PEG and PCL). The *in situ* gels exhibited G' of 50–200 kPa, adhesion strength of 40–90 kPa and gelation time as high as 8 minutes. Another adhesive system wherein chitosan backbone was conjugated with catechol (Chitoral) exhibited adhesion strength of 5–25 kPa against different oral tissues, however the G' exhibited was 0.1–1 kPa which upon incubation with water/saliva reduces to 0.0001–0.1 Pa.[47] Similar hydrogel formulation with catechol conjugated chitosan which crosslinks upon addition of genipin (G' – 0.01–1 kPa) has been reported.[48] None of these studies provide any evidence of cohesive failure upon removal despite the high adhesion strength, thus exposing the tissues to damage upon removal.

BC_PDz(h) adhesive composites reported here present several advantages such as (i) on-demand adhesion with crosslinking time as low as 15–60 seconds, (ii) covalent bond mechanism of adhesion, (iii) storage modulus of 1–10 kPa (measuring gap 0.45 mm) mimicking oral tissue, (iv) wet tissue adhesion strength of 3–35 kPa, (v) no harsh chemicals/oxidants required for crosslinking, (vi) reduced concentration of PDz in the composite thus reducing $-NH_2$ exposure to tissues. The BC_PDz(h) composites also exhibit adhesion strength similar to BC_PDz(lc) (7–17 kPa) systems evaluated in our previous paper.[19] The hydrogel system also allows for easy incorporation of biologics, cells and active ingredients into the matrix compared to films. However, several limitations of this technology are noted. The system requires further evaluation on the effects of applied UV dose on tunable adhesion properties. The effect of light penetration on mechanical properties of the composites could be further studied following recent findings of visible light activation of diazirine.[62] Lyophilized composite formulations are found to loose part of their material properties upon rehydration (6–9 times reduction in G' max, 2–3 times higher gelation dose, 6–10 times reduction in yield stress, Fig. S9, ESI†). Future work will evaluate the utility of the composites as drug depot and *in vivo* demonstrations of their application in oral cavity.

Conclusion

Aqueous adhesive composites of bacterial cellulose and carbene bioadhesives are formulated for liquid to solid transition and tissue adhesion within the oral cavity. Bacterial cellulose provides a nanofiber network to control moisture content and rheological properties before photocuring. A tunable adhesion strength of 3–35 kPa is observed on wet substrates and 8–70 kPa against dry biomaterials. The adhesion strength is variable depending on the composition and total solute percentage. Upon photo activation, the composites transform from viscous (liquid-like) state to elastic (solid-like) material properties in less than 60 seconds, providing rapid method of fixing films on tissue surfaces. Cohesive failure exhibited by the mucoadhesive patch prevents the damage of soft tissues in the oral mucosa upon removal. The light-activated composites present a new tool towards addressing unmet clinical needs in the oral cavity.

Conflicts of interest

The authors declare no conflicts of interest.

Acknowledgements

The project is partially supported by A*STAR IAF PP Grant (H19/01/a0/0II9): CathoGlu Bioadhesives-preventing catheter extravasation and skin infections; Ministry of Education Tier 2 Grant: CaproGlu, Double sided wet-tissue adhesives (MOE2018-T2-2-114).

References

1 S. L. James, D. Abate, K. H. Abate, S. M. Abay, C. Abbafati, N. Abbasi, H. Abbastabar, F. Abd-Allah, J. Abdela and A. Abdelalim, Global, regional, and national incidence, prevalence, and years lived with disability for 354 diseases

and injuries for 195 countries and territories, 1990–2017: a systematic analysis for the Global Burden of Disease Study 2017, *Lancet*, 2018, **392**(10159), 1789–1858.

2 V. Sankar, V. Hearnden, K. Hull, D. V. Juras, M. Greenberg, A. Kerr, P. Lockhart, L. Patton, S. Porter and M. Thornhill, Local drug delivery for oral mucosal diseases: challenges and opportunities, *Oral Dis.*, 2011, **17**(s1), 73–84.

3 S. Nguyen and M. Hiorth, Advanced drug delivery systems for local treatment of the oral cavity, *Ther. Delivery*, 2015, **6**(5), 595–608.

4 J. D. Smart, Theories of Mucoadhesion, *Mucoadhes. Mater. Drug Delivery Syst.*, 2014, 159–174.

5 S. B. De Souza Ferreira, T. D. Moço, F. B. Borghi-Pangoni, M. V. Junqueira and M. L. Bruschi, Rheological, mucoadhesive and textural properties of thermoresponsive polymer blends for biomedical applications, *J. Mech. Behav. Biomed. Mater.*, 2016, **55**, 164–178.

6 R. Shaikh, T. R. Raj Singh, M. J. Garland, A. D. Woolfson and R. F. Donnelly, Mucoadhesive drug delivery systems, *J. Pharm. BioAllied Sci.*, 2011, **3**(1), 89–100.

7 V. Hearnden, V. Sankar, K. Hull, D. V. Juras, M. Greenberg, A. R. Kerr, P. B. Lockhart, L. L. Patton, S. Porter and M. H. Thornhill, New developments and opportunities in oral mucosal drug delivery for local and systemic disease, *Adv. Drug Delivery Rev.*, 2012, **64**(1), 16–28.

8 I. S. Cho, H. M. Oh, M. O. Cho, B. S. Jang, J.-K. Cho, K. H. Park, S.-W. Kang and K. M. Huh, Synthesis and characterization of thiolated hexanoyl glycol chitosan as a mucoadhesive thermogelling polymer, *Biomater. Res.*, 2018, **22**(1), 30.

9 L. Mackaya-Navarro and V. H. Campos-Requena, Mucoadhesive alginate synthesis: a multivariate calibration approach, *New J. Chem.*, 2020, 20267–20274.

10 D. S. Jones, T. P. Laverty, C. Morris and G. P. Andrews, Statistical modelling of the rheological and mucoadhesive properties of aqueous poly(methylvinylether-*co*-maleic acid) networks: Redefining biomedical applications and the relationship between viscoelasticity and mucoadhesion, *Colloids Surf., B*, 2016, **144**, 125–134.

11 M. Pleguezuelos-Villa, A. Nácher, M. J. Hernández, M. A. O. V. Busó, M. Barrachina, N. Peñalver and O. Díez-Sales, A novel lidocaine hydrochloride mucoadhesive films for periodontal diseases, *J. Mater. Sci.: Mater. Med.*, 2019, **30**(1), 14.

12 T. Li, Q. Bao, J. Shen, R. V. Lalla and D. J. Burgess, Mucoadhesive *in situ* forming gel for oral mucositis pain control, *Int. J. Pharm.*, 2020, **580**, 119238.

13 L. Perioli, V. Ambrogi, F. Angelici, M. Ricci, S. Giovagnoli, M. Capuccella and C. Rossi, Development of mucoadhesive patches for buccal administration of ibuprofen, *J. Controlled Release*, 2004, **99**(1), 73–82.

14 R. Kumria, A. B. Nair, G. Goomber and S. Gupta, Buccal films of prednisolone with enhanced bioavailability, *Drug Delivery*, 2016, **23**(2), 471–478.

15 H. A. El Azim, N. Nafee, A. Ramadan and N. Khalafallah, Liposomal buccal mucoadhesive film for improved delivery and permeation of water-soluble vitamins, *Int. J. Pharm.*, 2015, **488**(1-2), 78–85.

16 B. Nutan, A. K. S. Chandel and S. K. Jewrajka, Liquid Prepolymer-Based *in Situ* Formation of Degradable Poly(ethylene glycol)-Linked-Poly(caprolactone)-Linked-Poly(2-dimethylaminoethyl)methacrylate Amphiphilic Conetwork Gels Showing Polarity Driven Gelation and Bioadhesion, *ACS Appl. Bio. Mater.*, 2018, **1**(5), 1606–1619.

17 J. Guo, W. Sun, J. P. Kim, X. Lu, Q. Li, M. Lin, O. Mrowczynski, E. B. Rizk, J. Cheng, G. Qian and J. Yang, Development of tannin-inspired antimicrobial bioadhesives, *Acta Biomater.*, 2018, **72**, 35–44.

18 J. Guo, W. Wang, J. Hu, D. Xie, E. Gerhard, M. Nisic, D. Shan, G. Qian, S. Zheng and J. Yang, Synthesis and characterization of anti-bacterial and anti-fungal citrate-based mussel-inspired bioadhesives, *Biomaterials*, 2016, **85**, 204–217.

19 J. Singh, N. C. S. Tan, U. R. Mahadevaswamy, N. Chanchareonsook, T. W. J. Steele and S. Lim, Bacterial cellulose adhesive composites for oral cavity applications, *Carbohydr. Polym.*, 2021, 118403.

20 D. Harris and J. R. Robinson, Drug delivery via the mucous membranes of the oral cavity, *J. Pharm. Sci.*, 1992, **81**(1), 1–10.

21 G. L. Chee, J. C. Yalowich, A. Bodner, X. Wu and B. B. Hasinoff, A diazirine-based photoaffinity etoposide probe for labeling topoisomerase II, *Bioorg. Med. Chem.*, 2010, **18**(2), 830–838.

22 L. Dubinsky, B. P. Krom and M. M. Meijler, Diazirine based photoaffinity labeling, *Bioorg. Med. Chem.*, 2012, **20**(2), 554–570.

23 G. Feng, I. Djordjevic, V. Mogal, R. O'Rorke, O. Pokholenko and T. W. Steele, Elastic Light Tunable Tissue Adhesive Dendrimers, *Macromol. Biosci.*, 2016, **16**(7), 1072–1082.

24 G. Wicaksono, I. Djordjevic, A. H. Shah and T. W. Steele, Photorheology of bioadhesive dendrimer polycaprolactone composites, *Polym. Test.*, 2019, **80**, 106099.

25 A. H. Shah, I. Djordjevic and T. W. Steele, Tertiary blends of PAMAM/PEG/PEG tissue bioadhesives, *J. Mech. Behav. Biomed. Mater.*, 2020, **101**, 103405.

26 F. Gao, I. Djordjevic, O. Pokholenko, H. Zhang, J. Zhang and T. W. Steele, On-demand bioadhesive dendrimers with reduced cytotoxicity, *Molecules*, 2018, **23**(4), 796.

27 M. Singh, H. S. Nanda, J. Y. H. Lee, J. K. Wang, N. S. Tan and T. W. J. Steele, Photocurable platelet rich plasma bioadhesives, *Acta Biomater.*, 2020, **117**, 133–141.

28 L. J. Fox, R. M. Richardson and W. H. Briscoe, PAMAM dendrimer-cell membrane interactions, *Adv. Colloid Interface Sci.*, 2018, **257**, 1–18.

29 R. Jevprasesphant, J. Penny, R. Jalal, D. Attwood, N. McKeown and A. D'emanuele, The influence of surface modification on the cytotoxicity of PAMAM dendrimers, *Int. J. Pharm.*, 2003, **252**(1-2), 263–266.

30 F. Esa, S. M. Tasirin and N. A. Rahman, Overview of Bacterial Cellulose Production and Application, *Agric. Agric. Sci. Procedia*, 2014, **2**, 113–119.

31 E. Trovatti, N. H. C. S. Silva, I. F. Duarte, C. F. Rosado, I. F. Almeida, P. Costa, C. S. R. Freire, A. J. D. Silvestre and C. P. Neto, Biocellulose Membranes as Supports for Dermal Release of Lidocaine, *Biomacromolecules*, 2011, **12**(11), 4162–4168.

32 H. M. C. Azeredo, H. Barud, C. S. Farinas, V. M. Vasconcellos and A. M. Claro, Bacterial Cellulose as a Raw Material for Food and Food Packaging Applications, *Frontiers in Sustainable Food Systems*, 2019, **3**, 7.

33 M. Singh, H. S. Nanda, R. D. O'Rorke, A. E. Jakus, A. H. Shah, R. N. Shah, R. D. Webster and T. W. Steele, Voltaglue Bioadhesives Energized with Interdigitated 3D-Graphene Electrodes, *Adv. Healthcare Mater.*, 2018, **7**(21), 1800538.

34 L. Gan, N. C. Tan, A. H. Shah, R. D. Webster, S. L. Gan and T. W. Steele, Voltage-activated adhesion through donor–acceptor dendrimers, *Macromolecules*, 2018, **51**(17), 6661–6672.

35 J. Ping, F. Gao, J. L. Chen, R. D. Webster and T. W. Steele, Adhesive curing through low-voltage activation, *Nat. Commun.*, 2015, **6**(1), 1–9.

36 C. A. Schneider, W. S. Rasband and K. W. Eliceiri, NIH Image to ImageJ: 25 years of image analysis, *Nat. Methods*, 2012, **9**(7), 671–675.

37 A. H. Shah, O. Pokholenko, H. S. Nanda and T. W. Steele, Non-aqueous, tissue compliant carbene-crosslinking bioadhesives, *Mater. Sci. Eng., C*, 2019, **100**, 215–225.

38 T. W. Steele, C. L. Huang, E. Nguyen, U. Sarig, S. Kumar, E. Widjaja, J. S. Loo, M. Machluf, F. Boey and Z. Vukadinovic, Collagen–cellulose composite thin films that mimic soft-tissue and allow stem-cell orientation, *J. Mater. Sci.: Mater. Med.*, 2013, **24**, 8.

39 T. T. H. Pham, S. V. Vadanan and S. Lim, Enhanced rheological properties and conductivity of bacterial cellulose hydrogels and aerogels through complexation with metal ions and PEDOT/PSS, *Cellulose*, 2020, **27**(14), 8075–8086.

40 H. S. Nanda, A. H. Shah, G. Wicaksono, O. Pokholenko, F. Gao, I. Djordjevic and T. W. J. Steele, Nonthrombogenic Hydrogel Coatings with Carbene-Cross-Linking Bioadhesives, *Biomacromolecules*, 2018, **19**(5), 1425–1434.

41 A. H. Shah, O. Pokholenko, H. S. Nanda and T. W. J. Steele, Non-aqueous, tissue compliant carbene-crosslinking bioadhesives, *Mater. Sci. Eng., C*, 2019, **100**, 215–225.

42 M. Singh, C. S. Yin, S. J. Page, Y. Liu, G. Wicaksono, R. Pujar, S. K. Choudhary, G. U. Kulkarni, J. Chen and J. V. Hanna, Synergistic voltaglue adhesive mechanisms with alternating electric fields, *Chem. Mater.*, 2020, **32**(6), 2440–2449.

43 S. A. Fleming, Chemical reagents in photoaffinity labeling, *Tetrahedron*, 1995, **51**(46), 12479–12520.

44 S. Rençber, S. Y. Karavana, F. F. Yilmaz, B. Eraç, M. Nenni, H. Gurer-Orhan, M. H. Limoncu, P. Güneri and G. Ertan, Formulation and evaluation of fluconazole loaded oral strips for local treatment of oral candidiasis, *J. Drug Delivery Sci. Technol.*, 2019, **49**, 615–621.

45 S. S. Moreira-Oliveira, L. Amaral-Machado, W. N. De Oliveira, É. N. Alencar, K. C. Zatta, L. B. F. C. De Souza, A. D. C. Medeiros, G. M. Chaves and E. S. T. Egito, Buccal Bullfrog (Rana catesbeiana Shaw) Oil Emulsion: A Mucoadhesive System Intended for Treatment of Oral Candidiasis, *Pharmaceutics*, 2018, **10**(4), 257.

46 R. A. Baus, F. Zahir-Jouzdani, S. Dünnhaupt, F. Atyabi and A. Bernkop-Schnürch, Mucoadhesive hydrogels for buccal drug delivery: In vitro-in vivo correlation study, *Eur. J. Pharm. Biopharm.*, 2019, **142**, 498–505.

47 J. H. Ryu, J. S. Choi, E. Park, M. R. Eom, S. Jo, M. S. Lee, S. K. Kwon and H. Lee, Chitosan oral patches inspired by mussel adhesion, *J. Controlled Release*, 2020, **317**, 57–66.

48 J. Xu, S. Strandman, J. X. X. Zhu, J. Barralet and M. Cerruti, Genipin-crosslinked catechol-chitosan mucoadhesive hydrogels for buccal drug delivery, *Biomaterials*, 2015, **37**, 395–404.

49 M. Birch and P. Srodon, Biomechanical properties of the human soft palate, *Cleft Palate-Craniofacial J.*, 2009, **46**(3), 268–274.

50 R. W. Chan and I. R. Titze, Viscoelastic shear properties of human vocal fold mucosa: Measurement methodology and empirical results, *J. Acoust. Soc. Am.*, 1999, **106**(4), 2008–2021.

51 I. A. Rodríguez, M. T. López-López, A. C. X. Oliveira, M. C. Sánchez-Quevedo, A. Campos, M. Alaminos and J. D. G. Durán, Rheological characterization of human fibrin and fibrin–agarose oral mucosa substitutes generated by tissue engineering, *J. Tissue Eng. Regener. Med.*, 2012, **6**(8), 636–644.

52 S. Cheng, S. C. Gandevia, M. Green, R. Sinkus and L. E. Bilston, Viscoelastic properties of the tongue and soft palate using MR elastography, *J. Biomech.*, 2011, **44**(3), 450–454.

53 C. Castro, R. Zuluaga, J.-L. Putaux, G. Caro, I. Mondragon and P. Gañán, Structural characterization of bacterial cellulose produced by Gluconacetobacter swingsii sp. from Colombian agroindustrial wastes, *Carbohydr. Polym.*, 2011, **84**(1), 96–102.

54 A. Rebelo, A. Archer, X. Chen, C. Liu, G. Yang and Y. Liu, Dehydration of bacterial cellulose and the water content effects on its viscoelastic and electrochemical properties, *Sci. Technol. Adv. Mater.*, 2018, **19**, 203–211.

55 G. Feng, I. Djordjevic, V. Mogal, R. O'Rorke, O. Pokholenko and T. W. Steele, Elastic light tunable tissue adhesive dendrimers, *Macromol. Biosci.*, 2016, **16**(7), 1072–1082.

56 E. Oledzka, D. Kaliszewska, M. Sobczak, A. Raczak, P. Nickel and W. Kolodziejski, Synthesis and Properties of a Star-Shaped Poly (ε-Caprolactone)–Ibuprofen Conjugate, *J. Biomater. Sci., Polym. Ed.*, 2012, **23**(16), 2039–2054.

57 G. P. Sailema-Palate, A. Vidaurre, A. J. Campillo-Fernández and I. Castilla-Cortázar, A comparative study on Poly (ε-caprolactone) film degradation at extreme pH values, *Polym. Degrad. Stab.*, 2016, **130**, 118–125.

58 F. Gao, *On-demand bioadhesive hydrogel based on diazirine*, Doctoral, MSE Theses, Nanyang Technological University, DR-NTU, 2017.

59 Z. Wang, Slanted Functional Gradient Micropillars for Optimal Bioinspired Dry Adhesion, *ACS Nano*, 2018, **12**(2), 1273–1284.

60 H. B. P. Maya Davidovich-Pinhas, Methods to Study Mucoadhesive Dosage Forms, in *Mucoadhesive Materials*

and Drug Delivery Systems, ed. V. V. Khutoryanskiy, 2014, pp. 175–196.

61 N. A. Peppas and J. J. Sahlin, Hydrogels as mucoadhesive and bioadhesive materials: a review, *Biomaterials*, 1996, **17**(16), 1553–1561.

62 I. Djordjevic, G. Wicaksono, I. Šolić, J. Singh, T. S. Kaku, S. Lim, E. W. J. Ang, L. Blancafort and T. W. J. Steele, Rapid Activation of Diazirine Biomaterials with the Blue Light Photocatalyst, *ACS Appl. Mater. Interfaces*, 2021, **13**(31), 36839–36848.